JOURNAL OF AIRCRAFT
Vol. 47, No. 4, July–August 2010

Incorporation of Feedback Control into a High-Fidelity Aeroservoelastic Fighter Aircraft Model

Brian P. Danowsky* and Peter M. Thompson†
Systems Technology, Incorporated, Hawthorne, California 90250
Charbel Farhat‡ and Thuan Lieu§
CMSoft, Incorporated, Palo Alto, California 94303
and
Chuck Harris¶ and Jason Lechniak**
U.S. Air Force Flight Test Center, Edwards Air Force Base, California 93523

DOI: 10.2514/1.47119

Flight testing for aeroservoelastic clearance is an expensive and time consuming process. Large degree-of-freedom high-fidelity nonlinear aircraft models using computational fluid dynamics coupled with finite element models can be used for accurately predicting aeroelastic phenomena in all flight regimes including subsonic, supersonic, and transonic. With the incorporation of an active feedback control system, these high-fidelity models can be used to reduce the flight-test time needed for aeroservoelastic clearance. Accurate computational fluid dynamics/finite element models are computationally complex, rendering their runtime ill suited for adequate flight control system design. In this work, a complex, large-degree-of-freedom, transonic, inviscid computational fluid dynamics/finite element model of a fighter aircraft is fitted with a flight control system for aeroelastic oscillation reduction. A linear reduced-order model of the complete aeroelastic aircraft dynamic system is produced directly from the high-order nonlinear computational fluid dynamics/finite element model. This rapid runtime reduced-order model is used for the design of the flight control system, which includes models of the actuators and common nonlinearities in the form of rate limiting and saturation. The oscillation reduction controller is successfully demonstrated via a simulated flight test using the high-fidelity nonlinear computational fluid dynamics/finite element/flight control system model.

I. Introduction

AEROSERVOELASTIC (ASE) clearance for new and existing aircraft is a necessary yet very time consuming and expensive process. Aircraft envelope definition contains aeroelastic and aeroservoelastic boundaries that account for such phenomena as flutter, buffet, buzz, lightly damped response and limit cycle oscillations (LCO), among others. Because of the complexity of the aerodynamic fluid regime and the structure, computational fluid dynamic (CFD) and finite element models (FEM) that correctly characterize the behavior can become very high-order (millions of degrees of freedom) and are computationally intensive. Model complexity becomes increasingly more intense when it is required to correctly characterize nonlinear regions, such as highly viscous flows (e.g., insect flight and micro aerial vehicles) and the transonic regime (e.g., high-performance fighter aircraft and large transport aircraft). Model complexity of very high order, such as this, greatly inhibits its use for flight control system (FCS) design.

Aeroservoelasticity comprises the interaction between four dynamic disciplines: aerodynamics, structural dynamics (elastic and inertial), actuator dynamics, and an active FCS (Fig. 1). A complete dynamic model of the system must include the influence of each discipline, especially when the dominant frequencies of each system are within close proximity to each other. Traditional aeroelasticity, which includes aerodynamics, inertial, and elastic dynamics, neglects the actuator dynamics. It has been shown that in many cases the actuator dynamics cannot be neglected; higher-order [1] and even nonlinear [2] actuator models are often required to accurately characterize the complete ASE system.

The conventional approach to ASE testing [3–5] is analysis, followed by extensive ground tests, leading to flight tests. This approach is a requirement and will continue to be followed, even as better and more reliable computational methods evolve. More accurate analysis, in the form of improved computational models, will aid the experimental aspect of ASE certification. More reliable methods will predict more accurate ASE phenomena (e.g., flutter, LCO), making flight tests safer. Also, more accurate methods will most likely decrease the amount of flight testing needed for validation, bringing the cost down.

In addition to envelope clearance, ASE certification can require validating FCS designs, especially when these systems are tailored to avoid or take advantage of ASE phenomena (i.e., oscillation reduction control systems [6] and active aeroelastic wings [7–9]). A complex nonlinear ASE system model is ideal for describing the complete behavior of the aircraft. FCS design requires models of relatively low order and low complexity that can be simulated in near real time or faster. Unfortunately, the complexity and computational requirements of accurate CFD/FEM ASE models greatly inhibit their use for FCS design. Fortunately, modern model reduction techniques exist and are being further evolved to greatly reduce the order of the complex ASE models [10]. These reduced-order models (ROMs) retain the significant dynamic aspects of the full-order models and can be used for accurate FCS design. ROMs can be constructed from high-order models that are either linear or nonlinear.

A linear aeroelastic ROM contains a wealth of information in a very compact form. Not only can it be used as a means for much more rapid simulation but the linear ROM itself can be exploited in other ways. One use of the linear model is the prediction of stability (flutter) boundaries using completely analytical means. If input and

Presented as Paper 2009-5708 at the AIAA Atmospheric Flight Mechanics Conference, Chicago, IL, 10–13 August 2009; received 9 September 2009; accepted for publication 17 April 2010.

*Senior Research Engineer, 13766 S. Hawthorne Blvd. Senior Member AIAA.
†Chief Scientist, 13766 S. Hawthorne Blvd. Member AIAA.
‡Chief Scientist, 1900 Embarcadero Rd. Fellow AIAA.
§Research Scientist, 1900 Embarcadero Rd.
¶Aerospace Engineer, 412th Test Wing. AIAA Member.
**Aerospace Engineer, 412th Test Wing.

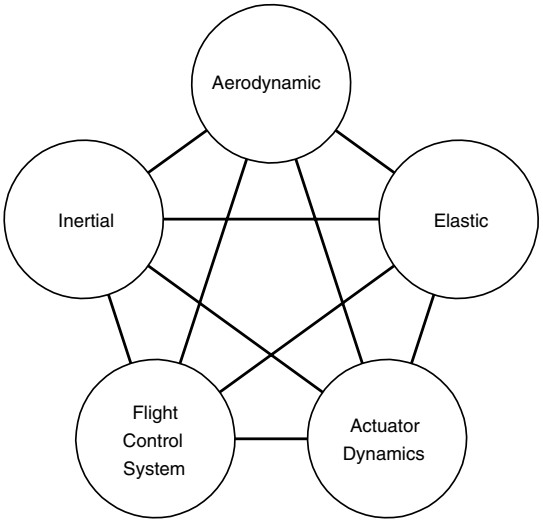

Fig. 1 Multidisciplinary ASE system.

output effectiveness derivatives are included with the ROM, classical flight control law design can be achieved. The ROM itself contains many important parameters pertaining to the flexible aircraft that can be extracted.

Recent research in the area of computational ASE analysis has used both linear and nonlinear aerodynamic models. A linear aeroservoelastic model of the X-29A aircraft was analyzed with active control and compared with experimental data [11]. Flutter suppression of an F-16-like wing using piezoelectric actuators was demonstrated using FEM and linear aerodynamic models [12]. Similarly, an aeroelastic F/A-18 aircraft model was fitted with a gust response reduction system using linear models [13]. More complex nonlinear aerodynamic models have also been demonstrated. A simplified pitch control augmentation system to address the residual pitch oscillation of a B-2 model that includes aerodynamic nonlinearities was demonstrated via simulation by Dreim et al. [14]. A flutter suppression control law was also implemented into a Euler-based CFD model of the Benchmark Active Controls Technology wing [15]. In the transonic regime, a flutter suppression control system for a missile was designed and demonstrated using linear ROMs [16]. The work presented herein follows these developing technologies by using high-fidelity CFD-based models for analysis, FCS design, and FCS implementation. The capabilities presented can be used for models of widely varying complexity, ranging from low-order aeroelastic models with linear potential flow based aerodynamics and linear structural dynamics to very high-order models with nonlinear full Navier–Stokes or Euler-based aerodynamics and nonlinear structural dynamics.

The objective of this work is to incorporate an active FCS into a complex high-order CFD/FEM ASE model of a high-speed fighter aircraft operating in the transonic flight regime. Simulations with a model of this caliber, including an active FCS, will produce results that will be representative of a system that is as close to reality as the complex model dictates. The objective is not limited to only simulating high-order ASE models with an active FCS but also to use the high-order models for FCS design. This includes producing a ROM directly from the high-order model that is capable of this task. The FCS is designed using this ROM rather than the full-order model. Subsequent simulated flight testing of the high-fidelity, high-order aircraft model with the FCS incorporated is the final step, providing full validation of the capabilities. The capability has the potential to aid subsequent flight testing, most likely reducing the amount of testing required, and thus making the flight testing process safer and cheaper.

II. Nonlinear Full-Order Model of the Aeroelastic High-Speed Fighter

The nonlinear full-order CFD/FEM model (NFOM) of the high-speed fighter is described in detail in [17] and is summarized here. The aerodynamic and elastic modeling is performed with the validated aeroelastic simulation code, AERO [18,19]. The aeroelastic computational model has two main components: 1) a FEM model that includes a representation of eight control surfaces: two flaps, two ailerons, two vertical rudders, and two stabilators and, 2) a dynamic CFD grid for inviscid, Euler flow computations.

A. Finite Element Base Structural Model

The base structural model built for aeroservoelastic applications is based on a previously verified FEM [20] that is composed of masses, springs, rigid beams, and flexible beams. The fuselage and wing structures of the fighter airframe are represented by several mass, beam, and spring elements that accurately represent the dynamic behavior. Various stores are also modeled by mass and beam elements and connected to the modeled wings by various stiff and flexible attachments.

B. Rigid Support Structure

The base structural model does not contain detail of the aerodynamic surface needed for accurate CFD calculations. To effectively communicate forces between the fluid and the structure, a rigid structure is implemented for the purpose of supporting a fictitious structural skin model that can communicate with the CFD surface mesh. This support structure, which extends to the stores and missiles, consists of massless rigid beam elements. Because of the absence of mass and stiffness, the incorporation of this support structure into the base FEM does not affect its dynamic properties (e.g., natural frequencies and mode shapes).

C. Phantom Structural Skin Model

The structural skin model designed for enabling the exchange of aerodynamic and elastodynamic data between the fluid and structural computational models consists of several phantom triangular elements. Phantom elements are elements with zero stiffness and mass properties. They are used to establish a data structure for communicating information between the CFD surface mesh and the structural surface model. A phantom element does not introduce any new nodes; it is specified using the nodes from the rigid support structure. Despite being massless with zero stiffness, a phantom element does not introduce singularities in the FEM computational solutions because it does not increase the model order.

D. Control Surface Deployment Mechanisms

Mechanisms for deploying the flaps, ailerons, and rudders are included in the FEM (Fig. 2). This slightly affects the stiffness properties of the base structural model as nodal splitting and torsional springs are introduced in the model to deploy the flaps, ailerons, rudders, and stabilators along their hinge lines. Surface deflections are initiated by the application of equal and opposite moments at specific node points on the base structure and control surface substructure that act along the control surface hinge lines.

E. CFD Euler Grid

The CFD grid is unstructured and suitable for inviscid (Euler) computations. It contains millions of tetrahedra and several hundred thousand grid points, many of which lie on the surface of the considered fighter configuration. The resolution of the CFD surface mesh far exceeds that of the structural phantom skin model since the fluid computations demand small control volumes for transonic calculations.

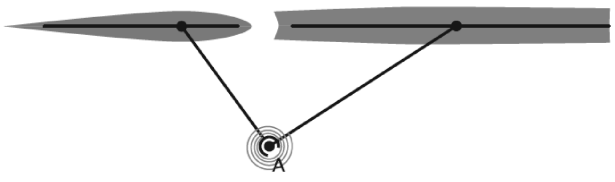

Fig. 2 Representation of the torsional spring actuation mechanism.

III. Linear Reduced-Order Model of the Aeroelastic High-Speed Fighter

The large degree-of-freedom NFOM requires parallel computing clusters for simulation and can take on the order of several days to run, prohibiting routine use for system analysis and control design. Fortunately, an established process has been evolved to produce a ROM that is several orders of magnitude smaller and still captures the vital dynamic characteristics of the full system. Simulations using the ROM can be performed several orders of magnitude faster than the full-order model and run on a standard desktop personal computer.

A number of ROM construction approaches have been under investigation for more than a decade. Beran has compiled a summary of modern ROM techniques [21]. One method seeks to use aerodynamic mode shapes of some linearized CFD solutions as a set of base vectors for order reduction. Other methods apply various system identification methods adopted from systems theory to identify a low-order model of the CFD-based aerodynamic system. Reduced-order model creation in all of these methods is computationally intensive [10], even in cases involving only a small number of full-order fluid response analyses to a small number of well-designed inputs. Yet, once such reduced-order models are created for a given configuration, dynamic simulation of many cases (corresponding to many inputs, dynamic pressures, and initial conditions) is fast and cheap computationally. It is expected that reduced-order aerodynamic methods will see increasing use in industry as part of the effort to create systems capable of analyzing large numbers of load cases and flight conditions using CFD-based aerodynamics.

The CFD/FEM code (AERO) used for the high-speed fighter configuration employs ROM building capabilities that compute linearized flow perturbations around an equilibrium solution, predict linearized aeroelastic responses assuming a modalized structure, generate snapshots for constructing a proper orthogonal decomposition (POD) basis, generate an aeroelastic ROM in the frequency domain, and compute aeroelastic ROM solutions in the time domain.

A. Governing Equations for the Aeroelastic System

The three-field arbitrary Lagrangian–Eulerian (ALE) can be used to represent the nonlinear aeroelastic system [22]. Semidiscretization by a finite volume method produces three coupled ordinary differential systems of equations [Eq. (1)]

$$\begin{aligned}(A(x)w)_{,t} + F(w, x, \dot{x}) &= 0\\ M\ddot{u} + f^{\text{int}}(u, \dot{u}) &= f^{\text{ext}}(u, w)\\ \tilde{K}x &= \tilde{K}_c u\end{aligned} \tag{1}$$

In the above equations A denotes the diagonal matrix composed of the fluid cell volumes, F is the nonlinear numerical flux function, w is the state vector of the fluid system, M is the FEM mass matrix, f^{int} is the vector of internal forces, f^{ext} is the vector of external forces and u is the vector of structural degrees of freedom. The fluid mesh deforms as the fluid-structure system interacts and its motion is described by the third equation above; the vector x represents mesh motion states where $\tilde{K}$ represents a fictitious stiffness matrix for describing the mesh motion and $\tilde{K}_c$ is a transfer matrix mapping mesh motion to structural displacements. The notation, t denotes the derivative with respect to time.

In short, a ROM is constructed by first linearizing these equations around an equilibrium point [23,24] nondimensionally [25]. The order is then reduced by defining a lower dimensional subspace via POD [21,26]. The POD method can be conducted in either the time domain or the frequency domain. For the purposes of this work, the ROM was constructed using POD in the frequency domain. The resulting aeroelastic ROM describes the equations of motion of the reduced fluid state vector w_r and the reduced structural state vector u_m outlined in the following sections. For a more comprehensive overview of the ROM construction process, the reader is referred to Lieu et al. [27].

B. Fluid ROM

The fluid ROM consists of an n_w order, POD-based, real, nondimensional, full square matrix ($\tilde{H}$), which governs the perturbed equations of the reduced fluid states about equilibrium. H is a dimensional square matrix that describes the behavior of the fluid states when dimensionalized by atmospheric properties. Equation (2) displays the linearized equations of motion with a dimensionalized ROM

$$\dot{w}_r = -Hw_r \tag{2}$$

In Eq. (2), w_r denotes the perturbation of the reduced-order fluid state vector about a steady state operating point; it is the perturbed, linearized and reduced approximation of w displayed in Eq. (1) above. The ROM matrix H has dimensions $n_w \times n_w$ and is dimensionalized as in Eq. (3)

$$H(p_\infty, \rho_\infty) = \tilde{H}\sqrt{p_\infty/\rho_\infty} \tag{3}$$

In Eq. (3), p_∞ and ρ_∞ denote the atmospheric pressure and density of interest, respectively. The ROM matrix can be exploited in at least the following ways: 1) this matrix can be used for a time-domain simulation assuming an appropriate initial condition is specified, and 2) H can be used to investigate the stability of the fluid system. If all real parts of the eigenvalues of $-H$ are negative, the fluid system is stable.

C. Aeroelastic ROM

The aeroelastic ROM consists of the fluid ROM combined with linearized structural dynamics. The coupled and scaled equations of motion are

$$\dot{w}_r + Hw_r + B\dot{u}_m + Cu_m = 0 \qquad I_m\ddot{u}_m + \Omega^2 u_m = Pw_r \tag{4}$$

In Eq. (4), u_m is an n_m length vector of structural modal displacements, Ω^2 is an $n_m \times n_m$ diagonal matrix composed of the squares of the natural structural frequencies, P is an $n_m \times n_w$ aerodynamic load transfer matrix, B and C are $n_w \times n_m$ fluid/structural coupling matrices, and I_m is the identity matrix of size m.

The coupled equations can be converted to a standard first-order state space form. The matrices, as shown, can be used for stability and initial condition response analysis. Not shown are the input and output coefficients needed for simulation and control analysis (these are described in the following section). The number of fluid and structural states can be changed as needed to improve validation (i.e., retain more structural modes). For a complete aircraft, typical numbers of structural modes needed to retain accuracy in frequency ranges of interest are five to 50. Because the fluid and structural states are separated in the form of Eq. (4), the structural equations can also be represented in a nonlinear form if desired without affecting the fluid state representation (i.e., in cases considering large structural deflections beyond elastic limits).

D. Inclusion of Input and Output Effectiveness with the ROM

The ROM represented by Eq. (4) does not contain any information defining the input/output relationship. The input and output effectiveness is needed for FCS design as well as open-loop simulations that include control surface deflections and sensor outputs. Inputs to the system are control surface deflections (in the form of equal and opposite moments that act along hinge lines) and outputs are sensor states (i.e., accelerations and rotational rates) at specific locations on the aircraft.

A generic aeroelastic system in terms of its inputs and outputs can be represented by Fig. 3. The system in the figure is general and can represent a linear or nonlinear system.

In Fig. 3, F_i represents a vector of the input forces at the specific structural node points and y_s represents a vector of the sensed outputs, which are states of specific structural node points. The node points used for the sensors are not necessarily the same as the node points used for the input forces.

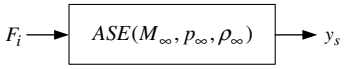

Fig. 3 Generic ASE input–output system.

The linearized reduced-order aerodynamic states and the structural modal states are represented by Eq. (4), which can also be represented by Eq. (5) below

$$\begin{aligned} &\dot{w}_r + Hw_r + \hat{B}X\dot{u}_m + \hat{C}Xu_m = 0 \\ &I_m\ddot{u}_m + \Omega^2 u_m = X^T F \quad \text{where}: B = \hat{B}X \quad \text{and} \quad C = \hat{C}X \end{aligned} \tag{5}$$

The matrix of retained structural mode shapes X, which is used to map the structural degrees of freedom to the modal domain, is introduced in this alternate representation. The forces acting on the structure have also been generalized to include any forces and moments acting on the structure F. This vector is a combination of forces from aerodynamics and other external forces.

The vector F, which represents the forces and moments acting on all structural degrees of freedom, can be separated into the aerodynamic forces [governed by the top of Eq. (5)] and a general vector of other external forces and moments (f) acting on all structural nodes:

$$F = \hat{P}w_r + f \quad \text{then} \quad X^T F = Pw_r + X^T f \quad \text{where}: P = X^T\hat{P} \tag{6}$$

The desired input vector F_i is composed of the equal and opposite moments that act at specific nodes on the structure to deploy control surfaces. These moments can be mapped to f linearly:

$$f = T_i^T F_i \tag{7}$$

The linear mapping matrix (T_i) is not square and will be mainly zero valued. Applying Eqs. (6) and (7) and ultimately to Eq. (5), will result in the coupled system with the augmented state vector defined as $q = [\, w_r \quad \dot{u}_m \quad u_m \,]^T$ and the inputs defined as F_i

$$\begin{aligned} &\dot{q} = Nq + GF_i \\ &\begin{bmatrix} \dot{w} \\ \ddot{u}_m \\ \dot{u}_m \end{bmatrix} = \begin{bmatrix} -H & -B & -C \\ P & 0 & -\Omega^2 \\ 0 & I & 0 \end{bmatrix} \begin{bmatrix} w \\ \dot{u}_m \\ u_m \end{bmatrix} + \begin{bmatrix} 0 \\ X^T T_i^T \\ 0 \end{bmatrix} F_i \\ &\text{where}, H \in \mathbb{R}^{n_w \times n_w} \\ &B \in \mathbb{R}^{n_w \times n_m} \qquad C \in \mathbb{R}^{n_w \times n_m} \qquad P \in \mathbb{R}^{n_m \times n_w} \qquad \Omega^2 \in \mathbb{R}^{n_m \times n_m} \\ &X^T T_i^T \in \mathbb{R}^{n_m \times n_i} \end{aligned} \tag{8}$$

The application of input effectiveness is completely described where inputs are defined as equal and opposite moments that act along the hinge lines of the control surfaces.

The sensors, in general, can be any structural node displacement, velocity or acceleration. A linear mapping can be determined that extracts the sensor nodes from the complete full degree-of-freedom structural displacement vector u. If the desired nodes are defined as u_d, the mapping matrix can be defined as T_s:

$$u_d = T_s u \tag{9}$$

By this definition the sensors, which are the displacement, velocity, and acceleration (both translational and rotational), can be described below:

$$\begin{aligned} y_s &= \begin{bmatrix} u_d \\ \dot{u}_d \\ \ddot{u}_d \end{bmatrix} = \begin{bmatrix} T_s & 0 & 0 \\ 0 & T_s & 0 \\ 0 & 0 & T_s \end{bmatrix} \begin{bmatrix} u \\ \dot{u} \\ \ddot{u} \end{bmatrix} \\ &= \begin{bmatrix} T_s X & 0 & 0 \\ 0 & T_s X & 0 \\ 0 & 0 & T_s X \end{bmatrix} \begin{bmatrix} u_m \\ \dot{u}_m \\ \ddot{u}_m \end{bmatrix} \end{aligned} \tag{10}$$

Expressing the sensors in the modal domain yields the third equality.

The output vector y_s can further be described as a linear function of the entire augmented state vector q and the input vector F_i [see Eq. (8) for $\ddot{u}_m$]

$$\begin{aligned} &y_s = Zq + DF_i \quad \text{where}, \qquad Z = \begin{bmatrix} 0 & 0 & T_s X \\ 0 & T_s X & 0 \\ T_s XP & 0 & -T_s X\Omega^2 \end{bmatrix}, \\ &D = \begin{bmatrix} 0 \\ 0 \\ T_s X X^T T_i^T \end{bmatrix} \qquad T_s X \in \mathbb{R}^{n_s \times n_m} \end{aligned} \tag{11}$$

With the input and the output defined, the complete linear state space system [Eq. (12)] is described by Eqs. (8) and (11)

$$\dot{q} = Nq + GF_i \qquad y_s = Zq + DF_i \tag{12}$$

The above system describes, in entirety, the input/output aeroelastic system displayed in Fig. 3 in a linearized form and is well tailored for FCS design.

IV. Design of the Active FCS for Oscillation Reduction Control

The large degree-of-freedom aeroelastic fighter aircraft has been described in a compact linear form that is suited for controller design. The aeroelastic system has many inputs and outputs. There are eight inputs that represent the eight control surfaces. For the model constructed, there were eight nodes selected as sensors. It is assumed that an inertial measurement unit is available at each sensor node that has access to six signals: three orthogonal translational accelerations and the three orthogonal rotational rates (i.e., representative of measurements taken from accelerometers and gyroscopes). The sensors are located at various points on the airframe: 1) center of mass, 2) nose (near the pilot), 3) left wing tip, 4) right wing tip, 5) left rudder tip, 6) right rudder tip, 7) left stabilator tip, and 8) right stabilator tip. Because each of the eight sensor locations has access to six signals, the total number of system outputs available is $8 \times 6 = 48$. With eight inputs the size of the input-output system is relatively large (48×8).

While it is possible to use all of the inputs and outputs for controller design, many of the inputs and outputs may not be necessary for the control task at hand. Using the minimum number of inputs and outputs will provide for a more simple design, making the designed FCS more efficient and elegant. For this work, the control task is oscillation reduction; therefore, it is desired to add damping to the natural response of the aircraft aeroelastic system. The system has many modes, some of which are sufficiently damped and will not require feedback control. Analysis of the open-loop dynamics reveals the problematic lower damped aeroelastic modes and provides information as to which inputs and outputs will be best at damping these problematic modes.

A. Analysis of Open-Loop Dynamics and Selection of Input and Output for Oscillation Reduction

For the following development, the ROM of the high-speed fighter aircraft corresponds to Mach 0.7 at an altitude of 10,000 ft. The ROM contains 18 structural states (9 structural modes and their derivatives) and 42 aerodynamic states. As stated previously, the ROM is

constructed nondimensionally for a fixed Mach number and dimensionalized according to atmospheric properties.

The open-loop eigenvalues of the ROM [N in Eq. (12)] are displayed in Fig. 4. The aeroelastic system at this altitude is stable but marginally so. Nine of the modes, which correspond to the aeroelastic structural modes, are the least damped, the fourth mode of which is very lightly damped. This is an asymmetric mode and the primary objective of the FCS is to provide sufficient damping to this mode. The system has the 8 inputs and 48 outputs available to damp this mode (and possibly some of the other modes). It is not necessary to use all inputs and outputs and it is desired to use as few inputs and outputs as possible. For simplicity and efficiency, a single-input-single-output (SISO) design is the most desired.

To determine which inputs and outputs will best damp this critical mode the time response residuals were compared. Time response residuals are the coefficients of the explicitly solved time-domain response of the system ($y_s(t)$) due to an impulsive input ($F_i = F_{i0}\delta(\tau)$). The ROM system is linear; therefore, the output time response $y_s(t)$, due to an input time series $F_i(t)$ and an initial state vector q_0, can be solved explicitly. If the initial state vector is assumed to be zero, the output time response due to an impulsive input (impulse at $t = 0$) is described by:

$$y_s(t) = Ze^{Nt}GF_{i0} \tag{13}$$

The system state dynamic matrix can be expressed in the modal domain [Eq. (14)]. In this form, the matrix N is expressed as a product of three square matrices: X_N is a matrix of the eigenvectors of N, $\Lambda = \mathrm{diag}(\lambda_1, \lambda_2, \ldots, \lambda_n)$ is a diagonal matrix of the eigenvalues of N and Y_N is the inverse of X_N

$$N = X_N \Lambda X_N^{-1} = X_N \Lambda Y_N \tag{14}$$

This form of N allows Eq. (13) to be expressed as a sum where each element in the sum is the sinusoidal response at each modal frequency

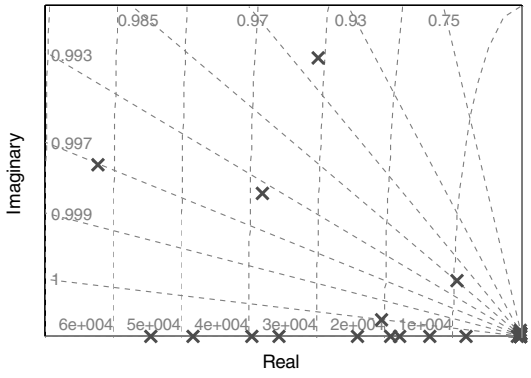

a) All eigenvalues

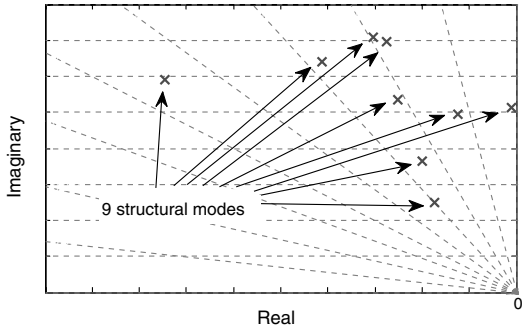

b) Detail around origin

Fig. 4 Aeroelastic airframe open-loop eigenvalues.

$$y_s(t) = Ze^{X_N \Lambda Y_N t}GF_{i0} = ZX_N e^{\Lambda t}Y_N GF_{i0} = \sum_{j=1}^{n} Zx_{Nj}y_{Nj}Ge^{\lambda_j t}F_{i0} \tag{15}$$

In the above equation, x_{Nj} is the jth column of X_N and y_{Nj} is the jth row of Y_N. The jth residual [Eq. (16)] is the relative amplitude of the time response corresponding to the jth mode at the jth frequency (eigenvalue magnitude)

$$AMP_j = Zx_{Nj}y_{Nj}G \tag{16}$$

The jth residual is a matrix which is the same size as the system (the number of outputs times the number of inputs). It is complex valued containing magnitude and phase information. There is a matrix AMP_j for each mode contained in X_N and these individual matrix elements display the relative effect of each input-output pair on that specific mode. For a given AMP_j, the element with the highest norm (expressed as, $\mathrm{sqrt}(\mathrm{Re}(AMP(i,k))^2 + \mathrm{Im}(AMP(i,k))^2)$) demonstrates that input k is the best at exciting the mode and output i is the best at measuring the mode.

Figure 5 displays the relative amplitudes of the elements of AMP_4, which corresponds to the least damped fourth mode. The 8 control surface inputs are along the x axis, the 48 sensor signals are along the y axis, and the norm of the elements of AMP_4 is displayed as individual bars with height along the z axis. The largest two elements of AMP_4 are clearly evident. These correspond to the nose lateral acceleration output ($\dot{v}_{\mathrm{nose}}$) due to aileron inputs ($\delta_{\mathrm{ail,left}}$ and $\delta_{\mathrm{ail,right}}$). The conclusion gathered from this analysis is that the fourth mode will be best controlled using the ailerons as inputs with feedback from the nose lateral acceleration sensor.

The above analysis reveals two inputs with essentially equivalent effect in magnitude. For further simplification, a differential aileron can be defined that maps the two inputs to one input [Eq. (17)]

$$\delta_{\mathrm{ail}} = \delta_{\mathrm{ail,left}} - \delta_{\mathrm{ail,right}} \tag{17}$$

The ailerons are each defined with positive deflection down; therefore this differential aileron input will command the left aileron down and the right aileron up, providing the traditional roll right aileron input. With the differential aileron defined this way, the controlled element aeroelastic system is SISO. The bare airframe root locus (detail around origin) is displayed in Fig. 6. The dynamics include a linear seventh-order actuator taken from [1].

B. Controller Design

With the SISO system defined as differential aileron in and nose lateral acceleration out, compensation to damp the fourth mode can be applied with traditional negative feedback (Fig. 7). Simple gain compensation will not be adequate as it will drive the fourth mode less stable. A fifth-order compensator (C) was designed to supply the sufficient damping. This compensator adds damping to the fourth mode as well as the second, sixth, and eighth modes, which are all asymmetric.

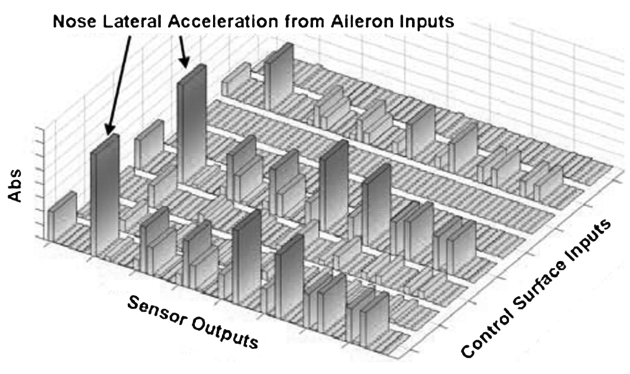

Fig. 5 Time response residual of the lightly damped fourth mode.

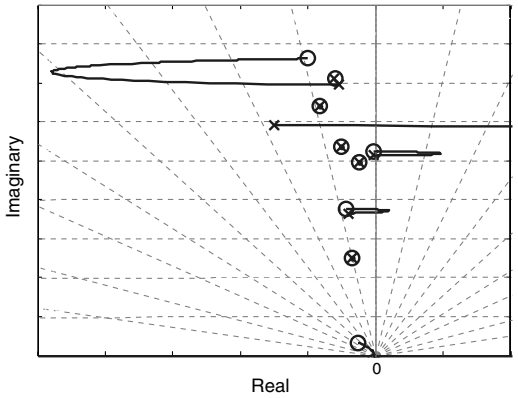

Fig. 6 Root locus for the bare flexible airframe ($\dot{v}_{nose}/\delta_{ail}$) including the aileron actuator.

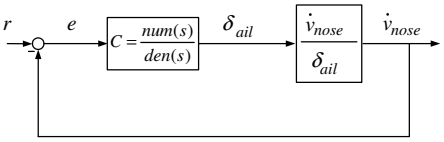

Fig. 7 Controller Structure.

A system survey of the designed compensator with the ROM is displayed in Figs. 8–12. It is immediately evident that the compensator effectively damps the fourth mode by both the closed-loop root locus (Fig. 8) and the initial condition response comparison (Fig. 9) in the survey. The input to system sensitivity (Fig. 10) displays the output of the compensator due to external inputs. The natural structural frequencies are also displayed in this plot and it is shown that input frequencies near the second, fourth, sixth, and eighth modes show a drop in gain. The compensator frequency response is displayed in Fig. 11 and the loop transfer function (including the compensator and the flexible aircraft) frequency response is displayed in Fig. 12. The loop transfer function frequency response displays the relative input effectiveness. It is the goal to keep this gain low throughout the frequency range as a means to avoid actuator nonlinearities (position and rate limits) and to retain control authority for maneuvering. The designed compensator achieves the goal of providing sufficient damping to the natural response and keeping control authority low.

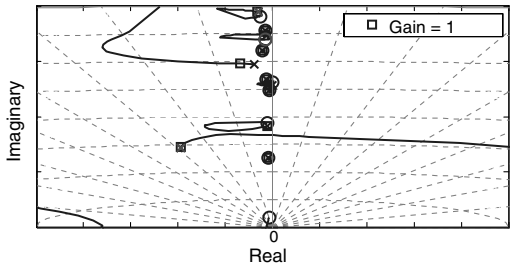

Fig. 8 System (plant and compensator) root locus.

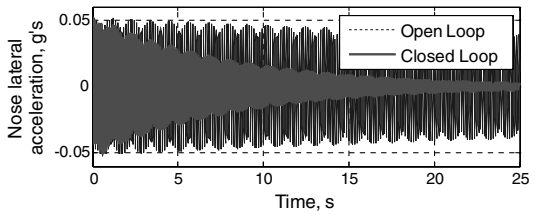

Fig. 9 Initial condition time response for open-loop and closed-loop systems.

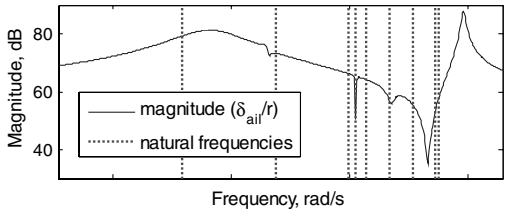

Fig. 10 Input to system sensitivity.

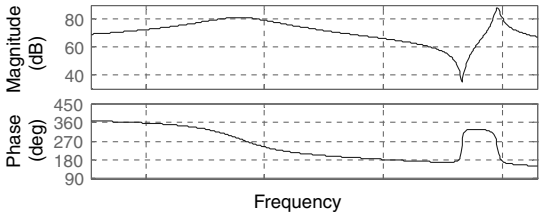

Fig. 11 Compensator frequency response.

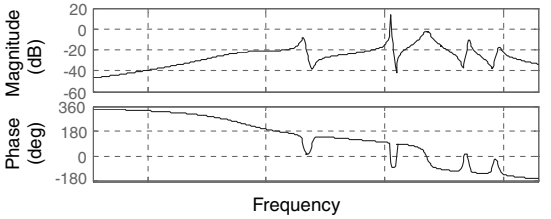

Fig. 12 Loop transfer function frequency response.

This controller represents a SISO design to achieve the objective of oscillation reduction. A controller with better performance and robustness can be designed using the ROM with multiple control surface inputs and multiple sensor outputs. The objective of this work is to demonstrate the feasibility of using very high-order complex aeroservoelastic aircraft models for controller design and implementation. Superior control design is not the focus; therefore controller complexity was kept minimal.

C. Demonstration of Controller Performance in the Presence of Actuator Nonlinearities with the ROM

Using the ROM, the controller executes with good performance. Nonlinearities arise due to the transonic nature of the flow regime which will not be represented by the linear ROM. Nonlinearities are also prevalent in other areas, namely the actuators. The actuators have position and rate limits that can, in some cases, cause instabilities with designed FCS. To verify the performance of the controller subject to these nonlinearities, simulations that include saturation and rate limits were conducted. It was assumed that the aileron actuators are limited to 100 deg/s rates and saturate when deflected $\pm 25°$. The compensator was designed to keep control authority low with these rate limit and saturation nonlinearities in mind.

Simulations were conducted using the ROM with applied rate limits and surface position limits using Simulink™. Rate and saturation limits were applied before being fed to the actuator to represent software rate limiting. Initially, the airframe is deflected in its fourth mode shape. The simulation was run in open-loop for the first 15 s, at which point the oscillation reduction controller is activated and continues to be active throughout the rest of the simulation. Figure 13 displays the nose sensor lateral acceleration and it is evident that the controller is supplying damping, even when the surface rate limits and saturation are present. Figure 14 displays the aileron position, which is maintained below 3.5° for the duration of the simulation. Figure 15 displays the aileron position rate. The rate limit is active from 15 to approximately 23 s. The acceleration

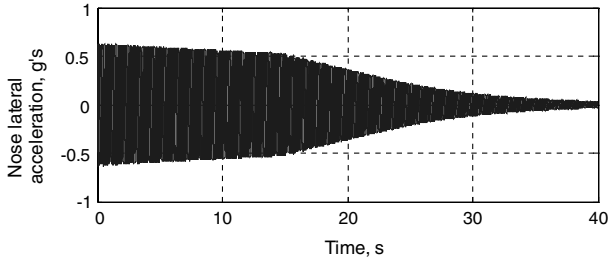

Fig. 13 Simulated nose lateral acceleration response using the ROM with controller activated at 15 s simulation time.

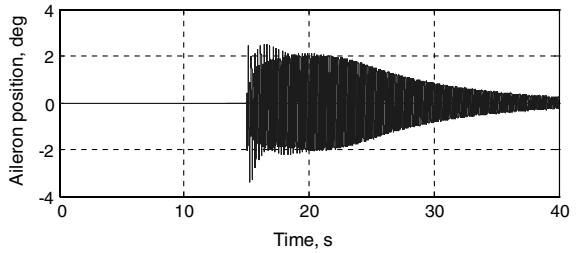

Fig. 14 Simulated aileron position using the ROM with controller activated at 15 s simulation time.

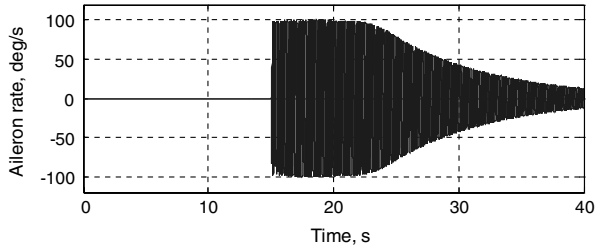

Fig. 15 Simulated aileron position rate using the ROM with controller activated at 15 s simulation time.

response displays no instabilities and adequate damping despite the presence of the active rate limit.

Using the linear ROM, the controller has been designed and performs as expected, even when subject to actuator nonlinearities. The final validation step is a simulated flight test with the controller and the full-order nonlinear flexible airframe model.

V. Validation of the Active FCS using the NFOM of the Aeroelastic High-Speed Fighter

The NFOM has been used to construct a linear ROM, which was then used to successfully design and implement an active oscillation controller. As a final validation step, the controller has been employed and implemented to be used with the CFD/FEM model to form the complete CFD/FEM/FCS model. The high-speed fighter is operating in the transonic flight regime, therefore complexities and nonlinearities associated with this fluid regime will be modeled and simulated.

A. General Controller Structure for Implementation with the NFOM

The AERO CFD/FEM model is equipped with the capability to internally output any structural nodal state (e.g., acceleration or rotational rate) for use with an internal function to produce outputs in the form of forces and moments that will act on any structural node at the next time step. The function that maps the nodal states to nodal forces is completely general and has been used to apply the FCS. The FCS, as designed using the ROM, outputs control surface hinge moments directly. This is well tailored for use with the full-order model. There is an inherent delay in the full-order model of exactly one time step, which is unavoidable with the current implementation. Although this introduces another potential source of error, it represents real-world computational and data transfer delays that exist in flight control systems on operational aircraft. The implementation of modern flight control systems in real-world aircraft is done almost exclusively digitally. Therefore, the implementation of the FCS used for validation with the NFOM was done in discrete time to represent that behavior of a digital FCS.

Significant generality was applied to the implementation of the FCS with the NFOM so that future FCS designs with completely different objectives could be applied with ease. As part of this generality, a standard control structure was defined (Fig. 16) complete with the compensator dynamics (Comp), actuator dynamics (Act), prefilter dynamics (Filt), sensor feedback dynamics (Sens) and the controllable element (Fighter). The inputs and outputs to the NFOM (u and y) with this structure can be multidimensional and the blocks that define the control system can be linear or nonlinear, allowing for control systems of low and high complexity. An external input r can also be supplied which can be used to test stability augmentation schemes with inputs (e.g., simulated stick and pedal inputs to validate flying qualities). The NFOM is blind to the makeup of the FCS so the controller structure can be represented alternatively as a single function (FCS) with y and r as inputs and u as the output (Fig. 17).

The NFOM views the actuator dynamics as part of the FCS so they must be incorporated in the FCS if they are to be considered. It was decided to supply the actuator dynamics in this fashion in anticipation of future developments. Implementation in this manner allows for different actuator models to be supplied more easily without affecting that CFD/FEM NFOM model.

The FCS was designed using tools built in the Matlab™/Simulink™ platform with this general control structure implemented. The tools take the components of the control system in Fig. 16 and autogenerate the source code needed for the AERO CFD/FEM model (FCS in Fig. 17). A testing platform has also been constructed in Simulink that uses the exact source code the NFOM uses. The exact FCS can then be tested with the ROM before a full-order system test for error checking. The full-order system tests can take on the order of several days to run so validated error free FCS code is of significant value.

B. Validation of FCS Performance via NFOM Simulation

The FCS was implemented within the full-order model as described above to form the complete CFD/FEM/FCS model. The NFOM simulation solves at each time-step the ALE form of the Euler equations [Eq. (1)], which includes an algebraic system for the flow solution and an algebraic system for solving the pseudostructural mesh motion solver. To excite the system, the airframe was initialized with a structure deflected in the fourth mode shape. For this demonstration the FCS is active throughout the duration of the simulation. Figures 18–20 display the nose lateral acceleration, the aileron position, and the aileron rate time histories, respectively. Figure 21

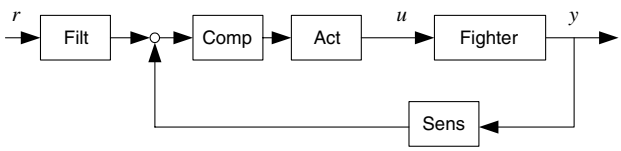

Fig. 16 General control system structure for use with the NFOM.

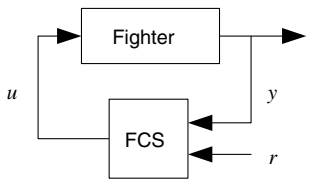

Fig. 17 Alternative representation of the control system.

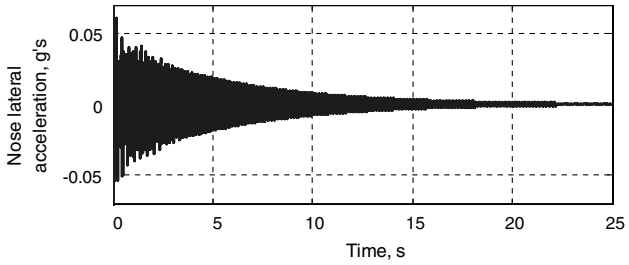

Fig. 18 Simulated nose lateral acceleration response using the NFOM.

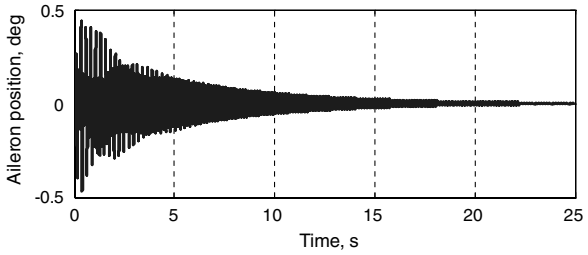

Fig. 19 Simulated aileron position using the NFOM.

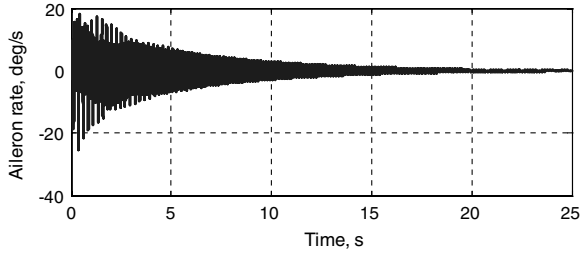

Fig. 20 Simulated aileron position rate using the NFOM.

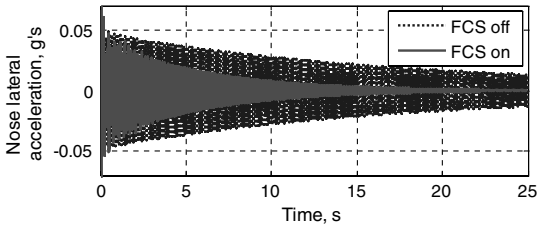

Fig. 21 Comparison of the nose lateral acceleration with and without an active FCS using the NFOM.

displays the comparison of two NFOM simulations: 1) with an active FCS and 2) without an active FCS. It is well evident that the FCS properly supplies damping to the response.

From the above figures it is apparent that the FCS is providing the adequate damping to the full-order nonlinear aeroelastic system. Figure 21 shows the comparison to the uncontrolled case. This plot displays that the amplitude of the oscillations at the nose acceleration sensor are being damped as expected. The simulation to generate this data with the nonlinear full-order model took approximately seven days and four hours to complete.[††]

VI. Conclusions

A very high-order combined CFD and FEM for an aeroservoelastic high-speed fighter aircraft has been used for FCS design and implementation, and a model that contains all aspects (CFD/FEM/FCS) has been successfully demonstrated. The considered high-performance fighter model used for this demonstration is operating in the transonic regime, displaying the efficacy of the methods for models of high complexity with inherent nonlinear behavior. The complex NFOM has been used directly to produce a linear ROM). This ROM has been successfully used for traditional system analysis and subsequent FCS design. Nonlinearities have been introduced in the actuators in the form of rate limiters and position saturations to test the robustness of the FCS in the presence of these real-world limits. The designed FCS has been implemented into a form that is interactive with the full-order model to produce the complete CFD/FEM/FCS model of the high-speed fighter. This full-order model has been used to complete simulated flight tests, demonstrating the capabilities and verifying the effectiveness of the designed FCS. The technology developed and demonstrated directly addresses the interaction between 1) complex structural/aerodynamic modeling and 2) FCS design and implementation. The high-fidelity CFD/FEM model has been used directly for FCS design as well as for full-order simulation with the imbedded FCS.

The degree of model fidelity that can be used with the developed technology is unbounded. Modeling complexity capability ranges from aeroelastic models with simple linear fluid dynamics (i.e., potential flow) to highly complex nonlinear fluid dynamics (i.e., Euler or full Navier–Stokes). Models operating in all flight regimes including subsonic, supersonic, and transonic are applicable. The ROM is produced directly from the full-order model, regardless of its inherent complexity, and accurately represents the dynamics of the system linearized around a defined operating point. This linear ROM is compatible with traditional linear system analysis, can be used for rapid simulation on a standard desktop platform, and does not require parallel computing clusters. These characteristics allow for traditional FCS design and implementation.

Acknowledgment

This work was conducted as part of a Phase II Small Business Innovation Research contract sponsored by the United States Air Force. The authors would like to thank the Air Force Flight Test Center at Edwards Air Force Base for valuable resources and funding to make this work possible.

AFFTC-PA-09316: Approved for public release; distribution is unlimited. This document is for information only. No US Government commitment to sell, loan, lease, codevelop or coproduce defense articles or provide defense services is implied or intended.

References

[1] Brenner, M. J., "Aeroservoelastic Modeling and Validation of a Thrust-Vectoring F/A-18 Aircraft," NASA TP-3647, Sept. 1996.

[2] Click, G. E., Henry, A. P., Rishel, R. L., Hager, J. W., McRuer, D. T., and Benun, D., "The Hydraulics System," Bureau of Aeronautics, Department of the Navy, Rept. AE-61-4 IV, March 1953.

[3] Kehoe, M. W., "AFTI/F-16 Aeroservoelastic and Flutter Flight Test Program-Phase-I," NASA TM 86027, 1985.

[4] Kehoe, M. W., "Aircraft Flight Flutter Testing at the NASA Ames-Dryden Flight Research Facility," NASA TM-100417, May 1988.

[5] Paduano, J. D., Feron, E., and Brenner, M., "Methods for In-Flight Robustness Evaluation," NASA CR-201886, Sept. 1995.

[6] Trame, L. W., Williams, L. E., and Yurkovich, R. N., "Active Oscillation Control on the F/A-18 Aircraft," AIAA Paper 85-1858, Aug. 1985.

[7] Voracek, D., Pendleton, E., Reichenbach, E., Griffin, K., and Welch, L., "The Active Aeroelastic Wing Phase I Flight Research Through January 2003," NASA TM-2003-210741, 2003.

[8] Cumming, S. B., and Diebler, C. G., "Active Aeroelastic Wing Aerodynamic Model Development and Validation for a Modified F/A-18A," AIAA Paper 2005-6312, Aug. 2005.

[9] Clarke, R., Allen, M. J., Dibley, R. P., Gera, J., and Hodgkinson, J., "Flight Test of the F/A-18 Active Aeroelastic Wing Airplane," AIAA Paper 2005-6316, Aug. 2005.

[10] Lieu, T., Farhat, C., and Lesoinne, M., "Reduced-Order Fluid/Structure Modeling of a Complete Aircraft Configuration," *Computer Methods in Applied Mechanics and Engineering*, Vol. 195, Nos. 41-43, 2006, pp. 5730–5742.

[††]Performed on a Dell PowerEdge cluster using 15 2.66 GHz cores.

doi:10.1016/j.cma.2005.08.026
[11] Gupta, K. K., Brenner, M. J., and Voelker, L. S., "Integrated Aeroservoelastic Analysis Capability with X-29A Comparisons," *Journal of Aircraft*, Vol. 26, No. 1, 1989, pp. 84–90. doi:10.2514/3.45726
[12] Schuster, D. M., Lieu, D. D., and Huttsell, L. J., "Computational Aeroelasticity: Success, Progress, Challenge," *Journal of Aircraft*, Vol. 40, No. 5, 2003, pp. 843–856. doi:10.2514/2.6875
[13] Nam, C., Chen, P. C., Liu, D. D., and Chattopadhyay, A., "ASTROS* with Smart Structures and ASE Modules:Application to Flutter Suppression and Gust-Load Alleviation," AIAA Paper 2000-1365, April 2000.
[14] Dreim, D. R., Jacobson, S. B., and Britt, R. T., "Simulation of Non-Linear Transonic Aeroelastic Behavior on the B-2," *Proceedings of the CEAS/AIAA/ICASE/NASA Langley International Forum on Aeroelasticity and Structural Dynamics 1999*, NASA CP-1999-209136, 1999, pp. 511–521.
[15] Stephens, C. H., Arena, A. S., Jr., and Gupta, K. K., "CFD-Based Aeroservoelastic Predictions with Comparisons to Benchmark Experimental Data," AIAA Paper 1999-766, Jan. 1999.
[16] Zhang, W., Ye, Z., and Zhang, C., "Aeroservoelastic Analysis for Transonic Missile Based on Computational fluid Dynamics," *Journal of Aircraft*, Vol. 46, No. 6, 2009, pp. 2178–2183. doi:10.2514/1.45249
[17] Thompson, P. M., Klyde, D. H., Farhat, C., and Harris, C., "Aeroservoelastic Predictive Analysis Capability," AIAA Paper 2007-6716, Aug. 2007.
[18] Farhat, C., Geuzaine, P., and Brown, G., "Application of a Three-Field Nonlinear Fluid-Structure Formulation to the Prediction of the Aeroelastic Parameters of an F-16 Fighter," *Computers and Fluids*, Vol. 32, No. 1, 2003, pp. 3–29. doi:10.1016/S0045-7930(01)00104-9
[19] Geuzaine, P., Brown, G., Harris, C., and Farhat, C., "Aeroelastic Dynamic Analysis of a Full F-16 Configuration for Various Flight Conditions," *AIAA Journal*, Vol. 41, No. 3, 2003, pp. 363–371. doi:10.2514/2.1975
[20] Goodman, C., Hood, M., Reichenbach, E., and Yurkovich, R., "An Analysis of the F/A-18C/D Limit Cycle Oscillation Solution," AIAA Paper 2003-1424, April 2003.
[21] Beran, P., "Reduced-Order Modeling: New Approaches for Computational Physics," AIAA Paper 2001-0853, Jan. 2001.
[22] Farhat, C., Lesoinne, M., and Maman, N., "Mixed Explicit/Implicit Time Integration of Coupled Aeroelastic Problems: Three-Field Formulation, Geometric Conservation And Distributed Solution," *International Journal for Numerical Methods in Fluids*, Vol. 21, No. 10, 1995, pp. 807–835. doi:10.1002/fld.1650211004
[23] Lesoinne, M., and Farhat, C., "CFD-Based Aeroelastic Eigensolver for the Subsonic, Transonic, And Supersonic Regimes," *Journal of Aircraft*, Vol. 38, No. 4, 2001, pp. 628–635. doi:10.2514/2.2839
[24] Lesoinne, M., Sarkis, M., Hetmaniuk, U., and Farhat, C., "A Linearized Method for the Frequency Analysis of Three-Dimensional Fluid/Structure Interaction Problems in all Flow Regimes," *Computer Methods in Applied Mechanics and Engineering*, Vol. 190, Nos. 24-25, 2001, pp. 3121–3146. doi:10.1016/S0045-7825(00)00385-6
[25] Lieu, T., "Adaptation of Reduced Order Models for Applications in Aeroelasticity," Ph.D. Thesis, Univ. of Colorado at Boulder, 2004.
[26] Thomas, J. P., Dowell, E. H., and Hall, K. C., "Three-Dimensional Transonic Aeroelasticity Using Proper Orthogonal Decomposition-Based Reduced Order Models," *Journal of Aircraft*, Vol. 40, No. 3, 2003, pp. 544–551. doi:10.2514/2.3128
[27] Lieu, T., Farhat, C., and Lesoinne, M., "Reduced-Order Fluid/Structure Modeling of a Complete Aircraft Configuration," *Computer Methods in Applied Mechanics and Engineering*, Vol. 195, Nos. 41–43, 2006, pp. 5730–5742. doi:10.1016/j.cma.2005.08.026